ChemSusChem

Research Article
doi.org/10.1002/cssc.202300945

Chemistry Europe
European Chemical Societies Publishing

www.chemsuschem.org

Special Collection

A Comparison of the Reactivity of the Lattice Nitrogen in Tungsten Substituted Co_3Mo_3N and Ni_2Mo_3N

Samia Al Sobhi,[a] Ihfaf AlShibane,[b] C. Richard A. Catlow,*[c, d, e] Angela Daisley,[b] Justin S. J. Hargreaves,*[b] Andrew L. Hector,*[a] Michael D. Higham,[c, d] and Constantinos D. Zeinalipour-Yazdi[f, g]

The effect of the partial substitution of Mo with W in Co_3Mo_3N and Ni_2Mo_3N on ammonia synthesis activity and lattice nitrogen reactivity has been investigated. This is of interest as the coordination environment of lattice N is changed by this process. When tungsten was introduced into the metal nitrides by substitution of Mo atoms, the catalytic performance was observed to have decreased. As expected, Co_3Mo_3N was reduced to Co_6Mo_6N under a 3:1 ratio of H_2/Ar. $Co_3Mo_{2.6}W_{0.4}N$ was also shown to lose a large percentage of lattice nitrogen under these conditions. The bulk lattice nitrogen in Ni_2Mo_3N and $Ni_2Mo_{2.8}W_{0.2}N$ was unreactive, demonstrating that substitution with tungsten does not have a significant effect on lattice N reactivity. Computational calculations reveal that the vacancy formation energy for Ni_2Mo_3N is more endothermic than Co_3Mo_3N. Furthermore, calculations suggest that the inclusion of W does not have a substantial impact on the surface N vacancy formation energy or the N_2 adsorption and activation at the vacancy site.

Introduction

In recent years there has been interest in the application of metal nitrides as heterogeneous catalysts for ammonia synthesis.[1] In this context, the origin of catalytic performance has been related to the operation of scaling relationships whereby metals which activate nitrogen strongly can be combined with those which activate nitrogen weakly such that catalytic performance can be tuned and indeed optimized.[2] This explanation has been advanced for the origin of the performance of Co_3Mo_3N, a nitride that possesses high activity as a catalyst for ammonia synthesis[3–7] and which has sometimes been described as a next generation catalyst. In this material, the combination of Mo, which activates nitrogen strongly, with Co, which activates nitrogen weakly, reportedly results in a material of better performance than the best single metal catalysts for ammonia synthesis.[2] Inherent in this rationalization of performance is the presence of the (111) surface plane where both Co and Mo are presented, with the lattice nitrogen in the Co_3Mo_3N phase not being active in itself, but rather being required to induce the correct crystallographic ordering such that the catalytically active surface plane is expressed.[2] An alternative mechanistic explanation for the activity of Co_3Mo_3N is that the lattice nitrogen is active and that ammonia synthesis occurs via a mechanism akin to the Mars-van Krevelen mechanism in which the hydrogenation of lattice nitrogen leads to the formation of ammonia as well as transient nitrogen vacancies which are the locus of nitrogen activation.[8] As summarized elsewhere, experimentally the reactivity of lattice nitrogen in Co_3Mo_3N has been demonstrated through its

[a] Dr. S. Al Sobhi, Prof. A. L. Hector
School of Chemistry
University of Southampton
Highfield, Southampton, SO17 1BJ (UK)
E-mail: a.l.hector@soton.ac.uk

[b] Dr. I. AlShibane, Dr. A. Daisley, Prof. J. S. J. Hargreaves
School of Chemistry
University of Glasgow
Glasgow, G12 8QQ (UK)
E-mail: justin.hargreaves@glasgow.ac.uk

[c] Prof. C. R. A. Catlow, Dr. M. D. Higham
Department of Chemistry, University College London
Kathleen Lonsdale Building,
Gower Place, London, WC1E 6BT (UK)
E-mail: c.r.a.catlow@ucl.ac.uk

[d] Prof. C. R. A. Catlow, Dr. M. D. Higham
Rutherford Appleton Laboratory
Research Complex at Harwell
Harwell, Oxon, OX11 0FA (UK)

[e] Prof. C. R. A. Catlow
School of Chemistry
Cardiff University
Park Place, Cardiff, CF10 1AT (UK)

[f] Dr. C. D. Zeinalipour-Yazdi
Computing, Mathematics, Engineering and Natural Sciences
Northeastern University London
London, E1W 1LP (UK)

[g] Dr. C. D. Zeinalipour-Yazdi
Department of Mechanical and Aerospaces
Brunel University London
London, Uxbridge, UB8 3PH (UK)

Supporting information for this article is available on the WWW under https://doi.org/10.1002/cssc.202300945

Special Collection This publication is part of a collection of invited contributions focusing on "Sustainable Ammonia Synthesis". Please visit chemsuschem.org/collections to view all contributions.

bulk reduction to form the Co_6Mo_6N phase, in which the retained lattice N relocates its crystallographic site, and also through isotopic exchange experiments, wherein temperature programmed heterolytic isotopic nitrogen exchange measurements have shown that a large proportion of the Co_3Mo_3N lattice nitrogen is exchangeable even in the absence of co-fed hydrogen.[8] Computational modelling has indicated that a significant concentration of surface lattice vacancies, which are effective for the activation of nitrogen, are present at temperatures of interest for catalytic ammonia synthesis[9] and modelling has also indicated the possibility of a novel associative ammonia synthesis mechanism occurring for Co_3Mo_3N;[10] a suggestion consistent with the low homomolecular nitrogen isotopic exchange performance of this material at temperatures where it is an effective ammonia synthesis catalyst.[8] The overall importance of nitrogen vacancies has subsequently been exemplified in novel highly active nitride-based ammonia synthesis catalysts such as Ni/LaN[11] and Ni/CeN.[12] On this basis, an enhanced understanding of the factors of importance in relation to the formation of nitrogen vacancies in nitride catalysts and modification of the local coordination environment of lattice nitrogen may aid the design and development of novel ammonia synthesis catalysts. In this paper, we build upon our previous work in relation to η-carbide[13] and filled β-Mn[14] structured ternary nitrides. We supplement some of our previous observations with experimental results in relation to local lattice N environment and also expand the range of systems which we have modelled with the aim of gaining new insight into which metal nitride formulations are more active for the ammonia synthesis reaction.

To date, experimental observations have demonstrated complex structure-activity and composition-activity relationships in the ternary nitride systems that we have investigated. As stated above, the η-6 structured Co_3Mo_3N system shows interesting reduction performance in the presence of hydrogen in that the η-12 structured Co_6Mo_6N phase, in which lattice N has relocated from the 16c to 8a Wyckoff crystallographic site, is formed. This results in a regenerable nitrogen looping reagent since some ammonia is produced in the process and the original phase can be restored using N_2 alone.[8] It is interesting, and perhaps surprising, to note that analogous behavior is not observed in the related isostructural Fe_3Mo_3N phase where, rather than leading to the lower nitrogen content phase, reduction at increasing temperature ultimately leads to structural decomposition.[15] Recent DFT modelling indicates the nitrogen formation energy to be more endothermic in the case of Fe_3Mo_3N than Co_3Mo_3N such that vacancy formation may be limited to the surface in the former case.[16] In the case of Ni_2Mo_3N, which possesses the filled β-Mn structure, no bulk reduction occurs upon treatment with hydrogen and, again, surface nitrogen vacancies have been proposed to be of possible importance.[17] Indeed, this material was observed to be particularly stable, with its phase being retained at temperatures up to 900 °C. The Ni metal sublattice of Ni_2Mo_3N has been progressively doped to make it more "cobalt-like" to see if this enhances bulk lattice nitrogen reactivity but in the isostructural $CoNiMo_3N$[18] and Co_2Mo_3N[15] materials, no bulk lattice N reactivity has been observed, as had also been the case for the latter material in studies reported by others.[19]

In summary, of all the systems that we have investigated to date, the bulk lattice nitrogen reactivity that we have observed in Co_3Mo_3N appears to be unique, which is possibly surprising since, in terms of first coordination environment, there is a significant similarity between the lattice N in Fe_3Mo_3N and Ni_2Mo_3N in that the lattice N is coordinated to 6 Mo species in all three phases. In the present study, we have extended the experimental work to determine the effect of doping the Mo sub-lattice of the Co_3Mo_3N and Ni_2Mo_3N systems with W to determine the effect of its modification of local nitrogen coordination environment. In relation to this, computational studies have been performed to explore the impact of tungsten doping on surface N vacancy formation, and N_2 adsorption and activation at surface N vacancy sites, both for the well-established Co_3Mo_3N phase as well as for the Ni_2Mo_3N system.

Experimental Section

For the $Ni_2Mo_{3-x}W_xN$ materials, a series of metal oxide precursors were prepared via a citrate gel process and were then converted to metal nitrides via ammonolysis as has been previously described for the $Ni_{2-x}Co_xMo_3N$ series.[17] $Ni(NO_3)_2.6H_2O$, $(NH_4)_6H_2W_{12}O_{40}.4H_2O$ and citric acid monohydrate (all obtained from Sigma-Aldrich) were employed. Ammonolysis was undertaken under flowing NH_3 at 800 °C for 12 h. The $Co_3Mo_{3-x}W_xN$ (x = 0.0, 0.1, 0.2, 0.3, 0.4, 0.5, 0.6, 0.7, 0.8 and 0.9) materials were synthesized using a similar procedure employing $Co(NO_3)_2.6H_2O$ (Sigma-Aldrich) as the cobalt source with ammonolysis being undertaken at 900 °C for 12 h due to the observation of mixed phase formation at lower temperature. Prior to reaction testing, samples were pre-treated under 60 mL min^{-1} of a 3:1 H_2/N_2 flow for 2 h at 700 °C to remove any passivation layer.

The lattice nitrogen reactivity was examined under 60 mL min^{-1} of a 3:1 ratio of H_2/Ar and at atmospheric pressure. The materials were first tested at 400 °C for 3 h, then the temperature was increased to 500 °C and maintained for 1 h 10 min. After, the temperature was increased to 600 °C and held for 1 h 10 min and finally the material was tested at 700 °C for 1 h 35 min. For the quantification of ammonia production, the vent gas was passed through a dilute sulfuric acid solution (0.00108 M) and the change in conductivity was monitored. This temperature programmed regime was applied to be consistent with our previous studies.

The ammonia synthesis activity tests were performed at atmospheric pressure and under a 60 mL min^{-1} flow of 3:1 H_2/N_2 with the production of ammonia being quantified by the decrease in conductivity of the standard 0.00108 M sulfuric acid solution through which the reactor effluent was flowed. The reaction testing was undertaken at 400 °C.

Powder X-ray diffraction (XRD) was obtained by using a PANalytical X-Pert Pro Diffractometer (40 kV, 40 mA) with a monochromatized CuK_α source ($\lambda = 0.154$ nm). The patterns were collected between 5–85° 2θ, with a step size of 0.0167° and a total scan time of 51 min. Rietveld analysis used the GSAS-2 package.[20]

CHN analysis of the materials was acquired by combustion on an Exeter Analytical Inc. CE-440 elemental analyzer.

The surface area of the pre-reaction samples was calculated by the Brunauer-Emmet-Teller (BET) method. The nitrogen adsorption/

desorption isotherms were carried out at liquid nitrogen temperature with a Micromeritics Tristar II surface area analyzer.

Scanning electron microscopy (SEM) and energy dispersive X-ray analysis (EDX) were performed using a Philips XL30-ESEM with a Thermofisher Ultradry detector and Noran System 7 analysis system.

Computational details: Models

Previous computational studies[9,10,16] have demonstrated the viability of the associative Mars-van Krevelen mechanism, which relies on the presence of surface N vacancies to serve as active sites for molecular N_2 adsorption. Hence, in the present work, we build on the models utilized in previous studies to explore the impact of W doping on the formation of surface N vacancies, and on N_2 adsorption and activation.

For the W-doped Co_3Mo_3N system, the impact of the presence of dilute W can be modelled by substituting a single Mo atom for W in the thin-film model used in the previous computational studies.[9,10] The model consists of a symmetric, asymmetric thin-film slab consisting of 3 N-containing layers, and terminated by a N-rich layer of the Co_3Mo_3N (111) surface (of stoichiometry $Co_{52}Mo_{48}N_{28}$), with a single Mo atom, coordinated with the surface N atoms, replaced by W (therefore having stoichiometry $Co_{52}Mo_{47}WN_{28}$), as illustrated in Figure 1. Whilst the use of a non-stoichiometric slab model prevents precise matching to the experimental stoichiometry, the model nonetheless provides a suitable starting point for investigating the impact of relatively low W concentrations (assuming that W is well-dispersed). The thin-film slab consists of a 2x2 surface supercell, to minimize lateral interactions between adsorbed species in adjacent periodic images, and three N-containing layers forming a non-stoichiometric symmetric slab model. The thin film slab was centered in the periodic cell, with a vacuum separation of 30 Å between slabs in adjacent periodic images, ensuring sufficient slab separation to avoid any spurious interactions.

For the Ni_2Mo_3N system, there are, to the authors' knowledge, no detailed previous computational studies investigating the mechanism of ammonia synthesis over Ni_2Mo_3N, with or without the inclusion of W. Whilst a detailed investigation of the comparative stability of different surface terminations of typical facets of Ni_2Mo_3N nanocrystals lies outside the scope of the present work, it is instructive to note the structural similarities between the η-carbide Co_3Mo_3N system, and the β-manganese Ni_2Mo_3N, and in particular the N-rich terminations of the (111) facet. In both cases, the N-rich termination exposes surface lattice N, which enables the formation of surface lattice N vacancies, with the surface lattice N coordinated with Mo, and with Mo_xN_y surface islands interspersed with Co or Ni clusters. Given that the N-rich terminated Co_3Mo_3N (111) thin film model was successfully used to provide valuable insights into the mechanism of ammonia synthesis over Co_3Mo_3N,[9,10] it is not unreasonable to assume that a similar model for Ni_2Mo_3N would likewise provide similarly useful information. Hence, thin film models were constructed for Ni_2Mo_3N and W-doped Ni_2Mo_3N analogously to that for Co_3Mo_3N (of stoichiometry $Ni_{32}Mo_{60}N_{28}$ and $Ni_{32}Mo_{59}WN_{28}$, respectively), as illustrated in Figure 2. Bulk optimization of Ni_2Mo_3N was performed by fitting the lattice parameter to the Birch-Murnaghan equation of state, with the resulting optimized lattice parameters being used to construct the Ni_2Mo_3N (111) surface thin film model, consisting of a 2x2 surface supercell and 3 N-containing layers, with thin films interleaved with 30 Å of vacuum.

Computational details: Methods

All calculations were performed using spin-polarized plane-wave density functional theory (DFT) as implemented in the VASP code (version 5.4.4).[21–23] During geometry optimization, all atomic positions were allowed to relax. In line with the previous computational studies for Co_3Mo_3N and Fe_3Mo_3N,[10,16] a Γ-centered (4×4×1) Monkhorst–Pack k-point sampling scheme was used for W-doped Co_3Mo_3N, Ni_2Mo_3N, and W-doped Ni_2Mo_3N, given the relatively similar dimensions of the 2x2 thin film surface supercells.[25] Inner electrons were replaced by projector-augmented waves (PAW),[26,27] and the valence states were expanded in plane-waves with a cut-off energy of 650 eV. The revised PBE (RPBE) exchange correlation functional was used throughout, with a dispersion correction applied using the D3 scheme devised by Grimme, and Becke-Johnson damping, in order to account for the weak van der Waals interactions responsible for physisorption behavior of species such as N_2.[28,29] No corrections were made to account for temperature and pressure effects; clearly, under real experimental conditions, such factors will have an impact on the vacancy formation process and N_2 adsorption, although these factors can at best only be approximated for a specific set of conditions. Moreover, the uncorrected DFT vacancy formation energies and N_2 adsorption energies can be directly compared with those reported in previous studies, providing greater insight into the behavior of similar systems, and the precise impact of W doping.

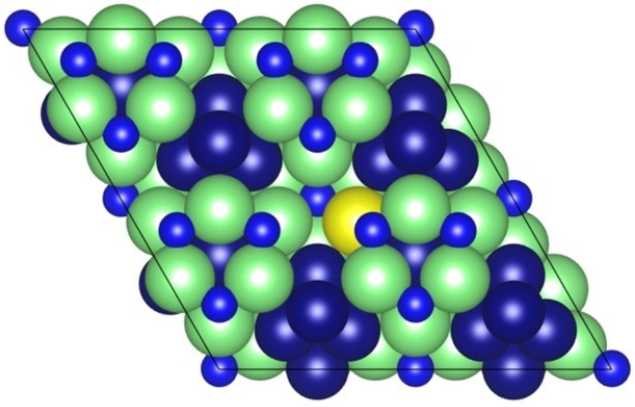

Figure 1. Graphic illustrating the model W-doped Co_3Mo_3N ($Co_{52}Mo_{47}WN_{28}$) surface. Key: Co, dark blue; Mo, green; W, yellow; N, pale blue.

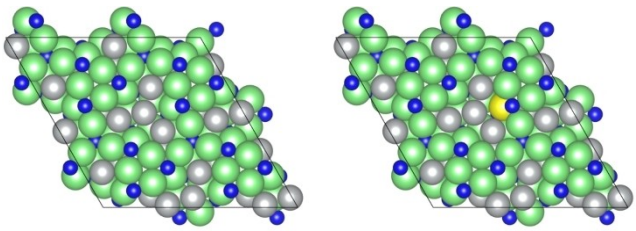

Figure 2. Graphic illustrating the Ni_2Mo_3N (111) thin film model (left) and the W-doped Ni_2Mo_3N (111) ($Ni_{32}Mo_{59}WN_{28}$) thin film model (right). Note the superficial similarity of the surface structure to the W-doped Co_3Mo_3N model (Figure 1). Key: Ni, grey; Mo, green; W, yellow; N, blue.

Results and Discussion

The powder X-ray diffraction (XRD) patterns of the materials tested in the current study are presented in Figure 3. It can be seen that the inclusion of a low level of tungsten in the sample has not produced any structural changes with the η-6 carbide structure with space group *Fd*3*m* being retained in the case of $Co_3Mo_{2.6}W_{0.4}N$ and the filled β-Mn structure with space group $P4_132$ for $Ni_2Mo_{2.8}W_{0.2}N$. The XRD results for a wider range of samples along with their lattice parameters are presented in the Supplementary Information (SI) file. In the SI file, the general increase in lattice parameter with increasing tungsten content up to a level of about $x = 0.3$ for $Ni_2Mo_{3-x}W_xN$ is evident as would be expected on the basis of Vegard's law taking into account the comparative size of W and Mo (Figure S13). Surprisingly, and reproducibly, the lattice parameter decreases in linear manner for $Co_3Mo_{3-x}W_xN$ up to about $x = 0.8$ as observed in Figure S5, the reason for this unexpected trend is currently obscure. All the materials tested were found to be active for ammonia synthesis (Table 1). $Co_3Mo_{2.6}W_{0.4}N$ and $Ni_2Mo_{2.8}W_{0.2}N$ were observed to have stable catalytic activity for 60 h (Figures S10 and S17) with post-reaction XRD showing no change in relation to their phase composition. The rates observed are lower than those reported in the literature which is consistent with the generally low surface areas of the materials (measured to fall within the range ca. 2–5 $m^2 g^{-1}$) possibly arising from the high temperatures applied during their preparation and it also appears that at initial sight, the inclusion of tungsten within the material is detrimental to performance. Whilst it is tempting to draw direct comparison between the relative performances of the nickel based and cobalt based systems particularly in view of their similar surface areas, caution should be exercised in this regard due to the differences in ammonolysis temperature employed since, for example, the role of morphology upon performance has not yet been established. This will be the subject of further investigation. Related W doped materials with a wider range of W doping have been tested for their catalytic activity for ammonia synthesis, albeit at a higher reaction temperature of 500 °C. The results are presented in Table S6 and are consistent with the general observations presented above.

In order to determine the reactivity of lattice nitrogen, samples were treated under a flow of 3:1 H_2/Ar in a temperature programmed regime as illustrated in Figure S9. In the case of the Co_3Mo_3N material the expected formation of Co_6Mo_6N occurs as observed in Figure 4 (although this is incomplete under the conditions investigated as shown by the presence of residual Co_3Mo_3N phase, possibly as a consequence of the low surface area of the material requiring longer time on line for quantitative transformation to be achieved). The loss of lattice nitrogen from the system was further verified on the basis of elemental analysis with the overall change being consistent with the formation of the mixed phase. Testing of the tungsten doped material was also demonstrative of the loss of lattice nitrogen with the formation of the nitrogen deficient phase being apparent from the XRD patterns shown in Figure 5, and the loss of nitrogen verified in terms of the data presented in Table 2. In relation to the reduction characteristics of the tungsten doped system, it is interesting to draw attention to previous studies of the binary W_2N nitride phase which have demonstrated it to be highly reducible generating a significant W phase component under conditions similar to those applied in the current study.[30] Tungsten doped Co_3Mo_3N has very recently been reported elsewhere, although its catalytic

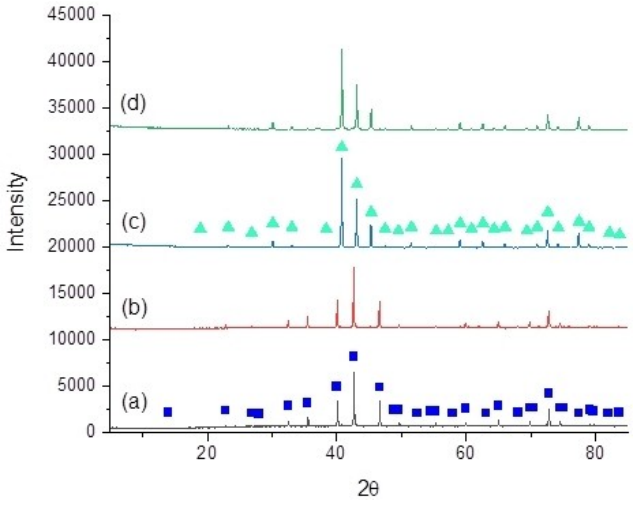

Figure 3. XRD patterns of: (a) Co_3Mo_3N, (b) $Co_3Mo_{2.6}W_{0.4}N$, (c) Ni_2Mo_3N and (d) $Ni_2Mo_{2.8}W_{0.2}N$. (○) Co_3Mo_3N and (△) Ni_2Mo_3N.

Table 1. Ammonia synthesis activity under 3:1 H_2/N_2 (60 mL min^{-1}) at 400 °C.

Material	Rate (μmol $h^{-1} g^{-1}$)	BET Surface Area ($m^2 g^{-1}$)	Specific Activity (μmol $h^{-1} m^{-2}$)
Co_3Mo_3N	58 ± 2	3	19 ± 1
$Co_3Mo_{2.6}W_{0.4}N$	20 ± 3	2	10 ± 2
Ni_2Mo_3N	114	3	38
$Ni_2Mo_{2.8}W_{0.2}N$	47 ± 6	4	12 ± 2

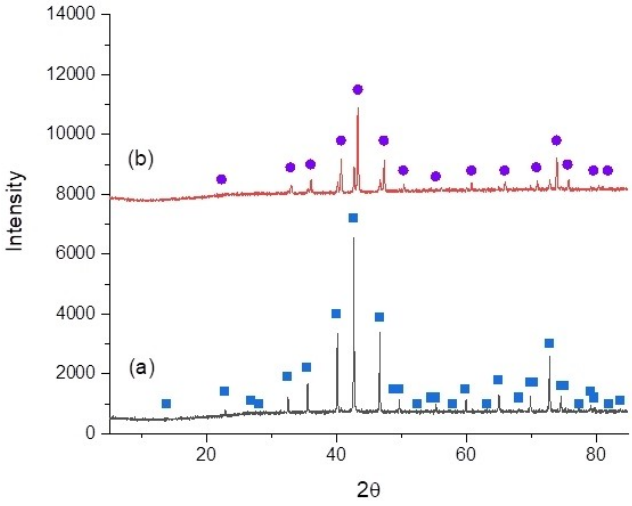

Figure 4. XRD patterns of Co_3Mo_3N: (a) pre-reaction and (b) post-reaction under 3:1 H_2/Ar at 400 °C–700 °C. (○) Co_3Mo_3N and (•) Co_6Mo_6N.

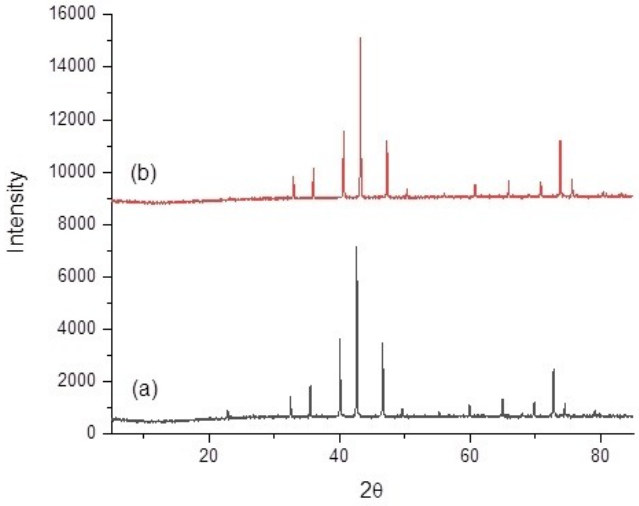

Figure 5. XRD patterns of $Co_3Mo_{2.6}W_{0.4}N$: (a) pre-reaction and (b) post-reaction under 3:1 H_2/Ar at 400 °C–700 °C. A shift in the position of the reflections to higher 2Θ with respect to pattern (a) corresponding to loss of lattice N can be seen in (b).

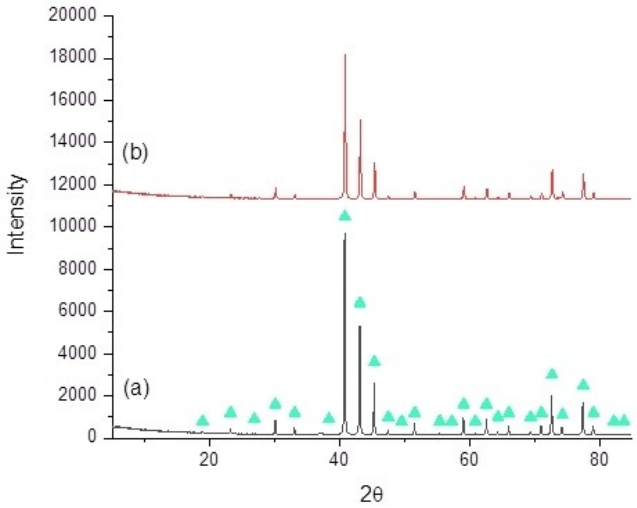

Figure 6. XRD patterns of Ni_2Mo_3N: (a) pre-reaction and (b) post-reaction under 3:1 H_2/Ar at 400 °C–700 °C. (△) Ni_2Mo_3N.

performance for ammonia synthesis and the reactivity of its lattice N was not reported.[31]

Consistent with our previous studies, Ni_2Mo_3N has been observed (Table 1) to be an effective ammonia synthesis catalyst,[17] although the bulk lattice nitrogen is resistant to reduction under the conditions applied within the current study (Figure 6). There does appear to be the loss of some nitrogen from the system on the basis of elemental analysis but this is not reflected in the powder diffraction patterns of the material before and after the reaction with H_2/Ar. Rietveld analysis of the diffraction patterns presented in the supplementary information indicated very little change in lattice parameters or other refined values (Figures S12 and S15). Again, the inclusion of a low level of tungsten appears to reduce the performance of the material for ammonia synthesis even though, on this occasion, its surface area is slightly increased. In line with the behavior of the parent phase, treatment of the tungsten doped sample under H_2/Ar under the conditions of the current study does not result in any apparent change in the reactivity of the bulk lattice nitrogen in the filled β-manganese structured system as shown in Figure 7.

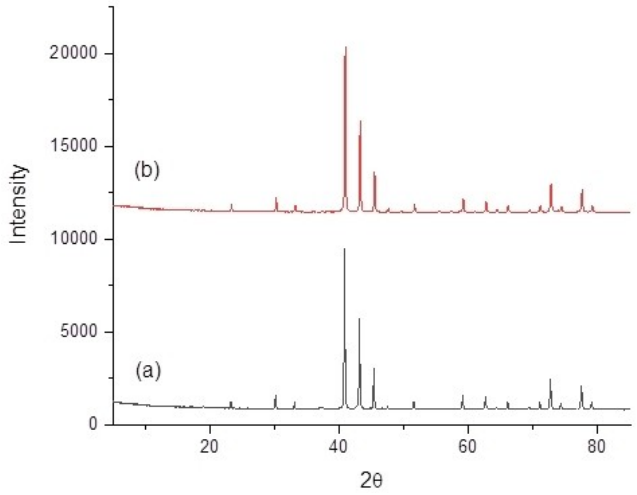

Figure 7. XRD patterns of $Ni_2Mo_{2.8}W_{0.2}N$: (a) pre-reaction and (b) post-reaction under 3:1 H_2/Ar at 400 °C–700 °C.

Computational Results: Surface N-vacancy formation

The associative Mars-van Krevelen mechanism for ammonia synthesis relies on the presence and regeneration of surface lattice N vacancies to facilitate N_2 activation, and its subsequent hydrogenation. Indeed, previous computational studies[10,16] determined surface N vacancy formation on Co_3Mo_3N and

Table 2. Elemental analysis for the nitrides pre- and post- reaction under 3:1 H_2/Ar at 400°C – 700°C.

Material	Pre-reaction nitrogen content (wt.%)	Post-reaction nitrogen content (wt.%)	Stoichiometric nitrogen content (wt.%)
Co_3Mo_3N	2.86	1.54	2.93
$Co_3Mo_{2.6}W_{0.4}N$	2.55	1.11	2.73
Ni_2Mo_3N	3.39	2.94	3.34
$Ni_2Mo_{2.8}W_{0.2}N$	3.27	3.16	3.21

Table 3. Calculated surface N vacancy formation energies (ΔE_{Vac}).

	Ni_2Mo_3N	$Ni_2Mo_{3-x}W_xN$	Co_3Mo_3N	$Co_3Mo_{3-x}W_xN$
ΔE_{Vac} (N_2)/eV	+2.90	+2.93	+1.68[10]	+1.60
ΔE_{Vac} (NH_3)/eV	+1.98	+2.01	+0.76	+0.68

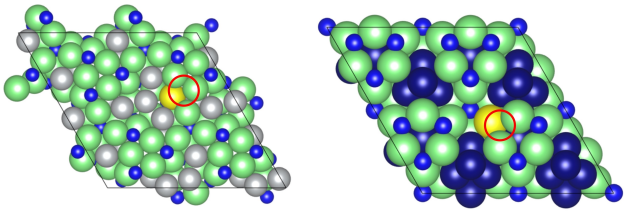

Figure 8. Graphic illustrating the presence of a surface N vacancy in the models used to represent W-doped Ni_2MoN ($Ni_{32}Mo_{59}WN_{28}$) (left) and W-doped Co_3Mo_3N ($Co_{52}Mo_{47}WN_{28}$) (right). Key: Ni, grey; Co, dark blue; Mo, green; W, yellow; N, pale blue. The red circle indicates the surface N vacancy site in both graphics.

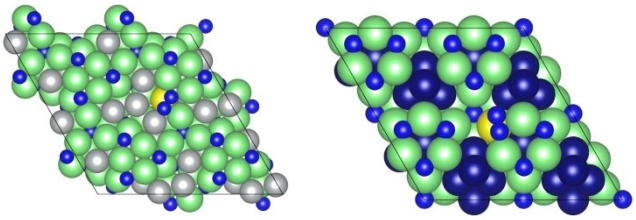

Figure 9. Graphic illustrating the adsorption of N_2 on a surface lattice N vacancy site for W-doped Ni_2Mo_3N ($Ni_{32}Mo_{59}WN_{28}$) (left) and W-doped Co_3Mo_3N ($Co_{52}Mo_{47}WN_{28}$) (right). Key: Ni, grey; Co, dark blue; Mo, green; W, yellow; N, pale blue.

Fe_3Mo_3N surfaces to be endothermic (both with respect to evolution of N_2, and NH_3 under hydrogenating conditions) at 0 K and under vacuum, but well within the bound of possibility under typical reaction conditions at finite temperatures and pressures. Hence, in the present work, it is of interest to determine the surface N vacancy formation energy for W-doped Co_3Mo_3N in order to compare with the previous results for the undoped Co_3Mo_3N system to assess the impact of the presence of W, and for both Ni_2Mo_3N and W-doped Ni_2Mo_3N to compare more generally with the previously studied ternary metal nitride systems. The calculations reveal that the presence of W does not appear to have a significant impact on the formation energy for a surface N vacancy, compared to the unpromoted systems. The formation energies are summarized in Table 3, whilst Figure 8 illustrates the optimized surface structures for a single N vacancy for the W-doped systems. The vacancy formation energies have been calculated both with respect to gaseous N_2, and with respect to NH_3 evolution under hydrogenating conditions. In all cases, the vacancy formation energy was determined to be endothermic, and considerably more so for Ni_2Mo_3N compared to Co_3Mo_3N, by approximately 1.3 eV. Even under hydrogenating conditions, the DFT-calculated vacancy formation energy for Ni_2Mo_3N is nearly 2 eV, suggesting that Ni_2Mo_3N is considerably more resistant to loss of lattice nitrogen than Co_3Mo_3N, in line with the experimental results. It must be noted, however, that the DFT-calculated vacancy formation energies do not account for factors such as contributions of temperature and pressure to the Gibbs free energy of vacancy formation, or the impact of entropy contributions associated with the consumption or evolution of gas phase species, or configurational entropy. Hence, it is possible but unlikely that surface N vacancies may be formed on Ni_2Mo_3N, but the calculations strongly suggest that their formation in appreciable concentrations would only occur at much higher temperatures than for Co_3Mo_3N.

The minimal impact of the presence of W on surface lattice N vacancy formation (less than 0.1 eV for both Ni_2Mo_3N and Co_3Mo_3N) is also consistent with the experimental results that suggest that the presence of W does not appear to have a significant impact on reactivity; if the reaction proceeds via an associative Mars-van Krevelen mechanism, as has already been explored for unpromoted Co_3Mo_3N,[10] a change in surface lattice vacancy concentration implies a change in concentration of active sites for N_2 activation, which would be expected to be reflected in the catalytic activity tests.

Computational results: N_2 adsorption and activation

Whilst the presence of W does not appear to have a significant impact on the formation of surface N vacancies in W-doped Ni_2Mo_3N or W-doped Co_3Mo_3N, it is of interest to consider if W enhances or inhibits N_2 adsorption and activation, which is a key prerequisite for the viability of the associative Mars-van Krevelen mechanism for ammonia synthesis. The results are presented in Table 4, with Figure 9 illustrating the adsorption geometry for activated N_2 at the vacancy site for W-doped Ni_2Mo_3N and W-doped Co_3Mo_3N. Once again, the results show that the impact of the presence of W on N_2 adsorption and activation at the vacancy site is minimal; in both cases, the

Table 4. Calculated N_2 adsorption energies ($\Delta E_{Ads.}(N_2)$) at the surface N vacancy sites, and N–N bond length(d) for the adsorbed N_2 molecule.

	Ni_2Mo_3N	$Ni_2Mo_{3-x}W_xN$	Co_3Mo_3N	$Co_3Mo_{3-x}W_xN$
$\Delta E_{Ads.}(N_2)$/eV	−2.75	−2.68	−0.73[10]	−0.88
d (N–N)/Å	1.36	1.37	1.30	1.25

presence of W changes the N_2 adsorption energy by no more than 0.13 eV. Whilst a slight elongation (by 0.01 Å) of the N_2 bond length is observed when W is present for Ni_2Mo_3N, for Co_3Mo_3N, the presence of W is accompanied by a slight reduction of the N–N distance (by 0.05 Å). Again, these calculations appear to be consistent with both the experimental results and the calculated vacancy formation energies. Likewise, the adsorption energy for N_2 on both Ni_2Mo_3N-based surface is considerably more exothermic than that for either of the Co_3Mo_3N-based surfaces, which is commensurate with the much more endothermic surface N vacancy formation energy, reflecting the inherent instability of the surface N vacancy site on Ni_2Mo_3N surfaces.

Computational modelling: Implications

The initial calculations presented here corroborate the experimental results, that suggest that the presence of W has a minimal impact on lattice nitrogen reactivity, and that lattice N is much more active in Co_3Mo_3N and related systems, compared to Ni_2Mo_3N and related systems. Whilst the calculations suggest the presence of W does not have a significant impact on the key initial processes involved in the associative Mars-van Krevelen mechanism for ammonia synthesis, this finding does not preclude W having an impact on the mechanism by inhibiting or enhancing subsequent elementary reaction processes. Indeed, the previous computational studies conducted for Co_3Mo_3N and Fe_3Mo_3N[10,16] suggest that the most energy-demanding processes involve the hydrogenation of surface lattice N to regenerate surface vacancies (or yield the second equivalent of NH_3 from adsorbed N_2). Hence, future computational studies will consider the complete reaction profiles for these systems in order to provide a more comprehensive perspective on the potential role of W on catalytic activity in candidate metal nitride systems for ammonia synthesis.

Conclusions

Co_3Mo_3N, $Co_3Mo_{2.6}W_{0.4}N$, Ni_2Mo_3N and $Ni_2Mo_{2.8}W_{0.2}N$ were examined for their ammonia synthesis activity and lattice nitrogen reactivity. The inclusion of tungsten in Co_3Mo_3N and Ni_2Mo_3N, which was undertaken to modify the local coordination environment of lattice N, was shown to lower the ammonia synthesis activity. However, $Co_3Mo_{2.6}W_{0.4}N$ and $Ni_2Mo_{2.8}W_{0.2}N$ were found to have similar lattice nitrogen reactivities to those of the corresponding unsubstituted nitride, with the lattice nitrogen in $Co_3Mo_{2.6}W_{0.4}N$ being highly reactive and a minimal loss of bulk lattice nitrogen observed for $Ni_2Mo_{2.8}W_{0.2}N$. The surface N vacancy site on Ni_2Mo_3N surfaces was calculated to be more unfavorable than for Co_3Mo_3N, with a higher vacancy formation energy by approximately 1.3 eV. The calculations show that the inclusion of tungsten does not have an effect on the formation energy of the surface N vacancy and the N_2 adsorption and activation at the vacancy site. The results imply that amongst this series of compounds, Co_3Mo_3N remains the most promising candidate system in terms of chemical looping for these ternary nitrides. Future studies will provide more in-depth investigation of the systems explored in the present work in order to more completely understand the impact of W doping and the precise role of Mo in facilitating N_2 activation in ternary metal nitride systems, with the intention of developing enhanced understanding leading to targeted materials design.

Acknowledgements

The authors would like to acknowledge the EPSRC for the research grants EP/T027851/1, EP/T028416/1 and EP/T028629/1 for the financial support of this project, and the UK Catalysis Hub Consortium (funded by EPSRC (Grants EP/R026815/1)) for the provision of additional resources. The authors acknowledge the STFC (SCARF) and UK National Supercomputing Service (ARCHER2) for the provision of computational resources, the latter enabled via membership of the MCC (EP/L000202).

Conflict of Interests

The authors declare no conflict of interest.

Data Availability Statement

The data that support the findings of this study are available from the corresponding author upon reasonable request.

Keywords: metal nitride · Mars-van Krevelen · DFT · nitrogen vacancies · ammonia synthesis

[1] J. S. J. Hargreaves, *Appl. Petrochem. Res.* **2014**, *4*, 3–10.
[2] C. J. H. Jacobsen, S. Dahl, B. S. Clausen, S. Bahn, A. Logadottir, J. K. Nørskov, *J. Am. Chem. Soc.* **2001**, *123*, 8404–8405.
[3] C. J. H. Jacobsen, *Chem. Commun.* **2000**, *12*, 1057–1058.
[4] R. Kojima, K-I. Aika, *Appl. Catal. A* **2001**, *215*, 149–160.
[5] R. Kojima, K-I. Aika, *Appl. Catal. A* **2001**, *218*, 121–128.
[6] R. Kojima, K-I. Aika, *Appl. Catal. A* **2001**, *219*, 157–170.
[7] R. Schlögl, *Angew. Chem. Int. Ed.* **2003**, *42*, 2004–2008.
[8] A. Daisley, J. S. J. Hargreaves, *Catal. Today* **2023**, *423*, 113874.
[9] C. D. Zeinalipour-Yazdi, J. S. J. Hargreaves, C. R. A. Catlow, *J. Phys. Chem. C* **2015**, *119*, 28368–28376.
[10] C. D. Zeinalipour-Yazdi, J. S. J. Hargreaves, C. R. A. Catlow, *J. Phys. Chem. C* **2018**, *122*, 6078–6082.
[11] T. N. Ye, S–W. Park, Y. F. Lu, J. Li, M. Sasase, M. Kitano, T. Tada, H. Hosono, *Nature* **2020**, *583*, 391–395.
[12] T. N. Ye, S–W. Park, Y. F. Lu, J. Li, M. Sasase, M. Kitano, T. Tada, H. Hosono, *J. Am. Chem. Soc.* **2020**, *142*, 14374–14383.
[13] D. Mckay, D. H. Gregory, J. S. J. Hargreaves, S. M. Hunter, X. Sun, *Chem. Commun.* **2007**, 3051–3053.
[14] T. J. Prior, P. D. Battle, *J. Solid State Chem.* **2003**, *172*, 138–147.
[15] A. Daisley, L. Costley-Wood, J. S. J. Hargreaves, *Top. Catal.* **2021**, *64*, 1021–1029.
[16] M. D. Higham, C. D. Zeinalipour-Yazdi, J. S. J. Hargreaves, C. R. A. Catlow, *Faraday Discuss.* **2023**, *243*, 77–96.
[17] N. Bion, F. Can, J. Cook, J. S. J. Hargreaves, A. L. Hector, W. Levason, A. R. McFarlane, M. Richard, K. Sardar, *Appl. Catal. A* **2015**, *54*, 44–50.
[18] S Al Sohi, N, Bion, J. S. J. Hargreaves, A. L. Hector, S. Laassiri, W. Levason, A. W. Lodge, A. R. McFarlane, C. Ritter, *Mater. Res. Bull.* **2019**, *118*, 110519.

[19] P. Adamski, D. Moszynski, M. Nadziejko, A. Komorowska, A. Sarnecki, A. Albrecht, *Chem. Pap.* **2019**, *73*, 851–859.
[20] B. H. Toby, R. B. Von Dreele, *J. Appl. Crystallogr.* **2013**, *46*, 544–549.
[21] G. Kresse, J. Hafner, *Phys. Rev. B* **1993**, *47*, 558–561.
[22] G. Kresse, J. Hafner, *Phys. Rev. B* **1994**, *49*, 14251–14269.
[23] G. Kresse, J. Furthmüller, *Comput. Mater. Sci.* **1996**, *6*, 15–50.
[24] G. Kresse, J. Furthmüller, *Phys. Rev. B* **1996**, *54*, 11169–11186.
[25] H. Monkhorst, J. Pack, *Phys. Rev. B* **1976**, *13*, 5188–5192.
[26] P. E. Blöchl, *Phys. Rev. B* **1994**, *50*, 17953–17979.
[27] G. Kresse, *Phys. Rev. B* **1999**, *59*, 1758–1775.
[28] S. Grimme, J. Antony, S. Ehrlich, H. Krieg, *J. Chem. Phys.* **2010**, *132*, 154104.
[29] S. Grimme, S. Ehrlich, L. Goerigk, *J. Comput. Chem.* **2011**, *32*, 1456–1465.
[30] A.-M. Alexander, Probing the reactivity of lattice nitrogen in transition metal nitrides, PhD thesis, University of Glasgow, **2011**.
[31] X. Gao, H. E. Bush, J. E. Miller, A. Bayon, I. Ermanoski, A. Ambrosini, E. B. Stechel, *Chem. Mater.* **2023**, *35*, 5864–5875.

Manuscript received: June 30, 2023
Revised manuscript received: August 25, 2023
Accepted manuscript online: September 13, 2023
Version of record online: October 9, 2023